SJMI(2019) 01; 11-23 ISSN : 2635-4608

DOI http://dx.doi.org/10.31916/sjmi2019-01-02

MR Weighted Image Discrimination by Artificial Intelligence

Giljae Lee, Gyehwan Jin, Hwunjae Lee, Jaeeun Jung

Received: 7 September 2019 / Accepted: 12 December 2019 / Published online: 30 December 2019

Abstract- In this study, we proposed a method of learning neural networks by optimizing neural network input parameters to discern MRI-weighted images. To this end, we segmented the weighting domain of MRI. In feature extraction, the original image and segmented image were extracted by DWT, respectively.

A neural network was trained by inputting extracted feature values. As a result of the experiment, it was found that the R-value of the segmented image is closer to 1 than the original image. The reason is that the images obtained by segmenting the areas of the weighted parts already have similarities. Also, it was found that the similarity between T1 and T2 weighted images is high in the same combination, and the similarity is relatively low in different weighted images. The most important issue in medical imaging is ensuring the confidence of radiologists using artificial intelligence. To solve this problem, it is of utmost importance that the algorithm developer and radiological technologist work together to provide a solution that is integrated with the radiologist's workflow.

Key word: Image processing, Discrete Wavelet Transform, MR pulse sequence, T2 Weighted Image, MR Molecular Imaging, Magnetic nanoparticles

GiljaeLee
The Korea Health Industry Development Institute
e-mail : korotkoff@khidi.or.kr

GeahwanJin(✉) ***corresponding author***
Dept. of Radiology, Nambu University
e-mail : ghjin@nambu.ac.kr

HwunjaeLee(✉) ***corresponding author***
YUHS-KRIBB Medical Convergence Research Institute
Dept.of Radiology, College of Medicine Yonsei University
e-mail : hjlee7@yuhs.ac.kr

Jaeeun Jung
Dept. of Radiological science, Daegu Health College
e-mail : :ejung@dhc.ac.kr

I. Introduction

Wilhelm Conrad Röntgen discovered a short-wavelength electromagnetic wave called X-rays on November 8, 1895,[1] and he won the 1901 Nobel Prize for Physics. For the first time in history, the discovery of X-rays provided the first advance in modern medicine by providing a

SJMI(2019) 01; 11-23

way to look inside the human body.

Recent medical images include Digital Radiography (DR), Computed Radiography (CR), Computed Tomography (CT), Positron Emission Tomography (PET), Single Positron Emission Tomography (SPECT), Ultra Sonography, and Magnetic Resonance Imaging (MRI).[2]

The World Economic Forum (WEF), chaired by Klaus Schwab, advocated the fourth industrial revolution in 2016[3]. The Fourth Industrial Revolution can be explained by a variety of new technologies that integrate the physical, biological and digital worlds based on big data and affect all sectors, including the economy, industry and healthcare.[3] The most impact of the 4th industry on medical care is the issue of big data-based artificial intelligence technology.

In this study, we propose a method of learning neural networks by optimizing neural network input parameters to discern MRI-weighted images. To this end, we segmented the weighting domain of MRI. In feature extraction, the original image and segmented image were extracted by DWT, respectively. A neural network was trained by inputting extracted feature values. If the feature extraction value is input and learned, the inference time of the AI will be reduced and the inference result will be accurate.

I. Materials and methods

1. Magnetic Resonance Imaging

Magnetic resonance imaging forms images by measuring patterns of hydrogen nuclei interacting with magnetic fields in magnetic fields and absorbing and emitting electromagnetic waves at specific frequencies.[4] About 70% of the human weight is body fluid, most of which is water. The proton, the nucleus of the hydrogen atom of water, has a spin in an arbitrary direction, and when it enters a strong magnetic field, the spin direction of the hydrogen nucleus is aligned along the direction of the magnetic field. In this state, when a high-frequency electromagnetic pulse is applied in a vertical direction, the hydrogen nucleus absorbs the energy of electromagnetic waves and changes the spin in the opposite direction of the magnetic field.[4] After that, when the pulse is broken, the hydrogen nucleus with reverse spin returns to its original state, releasing weak electromagnetic waves.[4] This electromagnetic wave can be detected to track and image the position of the hydrogen atom nucleus from which the electromagnetic wave is emitted. The relaxation time at which the hydrogen nucleus with reverse spin returns to its original state has two values, 'T1' and 'T2', depending on the relaxation coefficient of the spin. The relaxation of the spin of the hydrogen nucleus by interaction with the spin of the surrounding hydrogen nucleus is called spin-spin relaxation, and the time constant thereof is called T2.[4] In contrast, the relaxation of spin by interaction with the lattice structure of the surrounding tissue is called spin-lattice relaxation, and this time constant is called T1. T1 and T2 differ greatly depending on the surrounding tissues of the hydrogen nucleus, and the magnetic resonance image makes this relaxation time planar image[4]. Figure 1 shows a model of the MRI scanner and Figure 2 shows the images acquired by the MRI scanner. MRI images used in the experiment were obtained from The Cancer Imaging Archive. The obtained image was adjusted to 256 X 256 pixels, and the shape of the

image was transformed into a bit map (* .bmp) form.

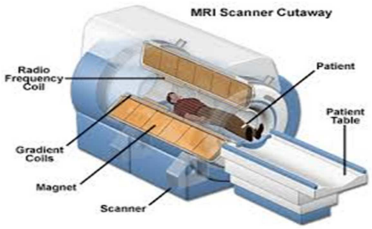

Figure 1. MRI Scanner[https://www.javatpoint.com/mri-full-form]

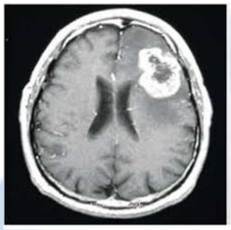

Figure 2. Brain Image

2. Image segmentation

In digital image processing, image segmentation is the process of dividing a digital image into segments. The goal of segmentation is to simplify or change the representation of the image to something more meaningful and easier to analyze.[5][6] Image segmentation is commonly used to find objects and boundaries (lines, curves, etc.) in an image. More precisely, image segmentation is the process of assigning a label to every pixel in an image so that pixels with the same label share specific characteristics. The result of the image segmentation is a set of segments that collectively covered with a set of contours extracted from the whole image or the image.[5][6] Each pixel in the area is similar in terms of some characteristics or calculated properties, such as color, intensity, or texture. Adjacent region varies considerably concerning for to the same characteristics.[7] When applied to image stacks, usually in medical imaging, contours created after image segmentation can be used to create 3D reconstructions using an interpolation algorithm such as the Marching cube.[8] Machine vision is a technology and method commonly used in the industry to provide imaging-based automated inspection and analysis for applications such as automated inspection, process control, and robot guidance.[9] Machine vision refers to many technologies, software and hardware products, integrated systems, operations, methods, and expertise. Machine vision in the field of systems engineering can be considered distinct from computer vision, a form of computer science.[9] We want to solve real problems by integrating and applying existing technologies in new ways. This term is widely used for these functions in industrial automation environments, but it is also used for these functions in other environments such as security and vehicle guidance. The whole machine vision process involves planning the requirements and details of the project and then creating a solution. During run time, the process starts with imaging and then automatically analyzes the image and extracts the necessary information.[10] The simplest method of image segmentation is called the threshold method. This method converts grayscale images to binary images based on the clip level. The key to this method is to choose a threshold. Several popular methods are used in the industry, including the maximum entropy method, the balance histogram threshold, the Oats method (maximum variance), and the k-mean clustering.[11] Recently, a method for

thresholding computed tomography (CT) images has been developed. The key idea is that, unlike Otsu's method, the threshold is derived from the radiograph instead of the (reconstructed) image.[12][13] The new method suggested the use of multidimensional fuzzy rule-based nonlinear thresholds. In these works, the determination of the membership of each pixel for a segment is based on multidimensional rules derived from fuzzy logic and evolutionary algorithms based on the image lighting environment and application.[14]

3. Discrete Wavelet Transform(DWT)

Wavelet transform was proposed in the mid-1980s, and it has been used in various fields such as signal processing, image processing, computer vision, image compression, biochemistry medicine, etc.[15] For image processing, it provides an extremely flexible multi-resolution image and can decompose an original image into different subband images including low- and high-frequencies. Therefore people can choose the specific resolution data or subband images upon their demands.[16] A 2-D DWT of an image is illustrated in Figure 3(a). When the original image is decomposed into four-subband images, it has to deal with row and column directions separately. First, the high-pass filter G and the low-pass filter H are exploited for each row data, and then are down-sampled by 2 to get high- and low-frequency components of the row. Next, the high- and the low-pass filters are applied again for each high- and low-frequency components of the column, and then are down-sampled by 2. By way of the above processing, the four-subband images are generated: HH, HL, LH, and LL. Each subband image has its feature, such as the low-frequency information is preserved in the LL-band and the high-frequency information is almost preserved in the HH-, HL-, and LH-bands. The LL-subband image can be further decomposed in the same way for the second level subband image.[17] By using 2-D DWT, an image can be decomposed into any level of subband images, as shown in Figure 3(b).

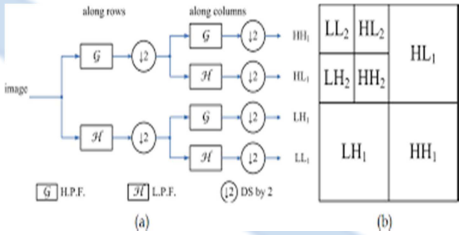

Figure 3. Diagrams of DWT image decomposition: (a) the 1-L 2-D analysis DWT image decomposition process, (b) the 2-L 2-D analysis DWT subband.

4. Artificial Intelligence in Medicine

Artificial intelligence (AI) has led to many medical advancements, from AI-based software for the management of medical records to diagnosing and recognizing conditions. Most of the new work on artificial intelligence in the medical field is related to diagnostic technology, and AI systems are trained to recognize the characteristics of various conditions.[18][19] Through ‘machine learning’ (ML), AI provides techniques that uncover complex associations that cannot easily be reduced to an equation.[20] For example, neural networks represent data through vast numbers of interconnected neurons in a similar fashion to the human brain. This allows ML systems to approach complex problem solving just as a clinician might by carefully weighing evidence to reach reasoned conclusions.[21] However, unlike a single

clinician, these systems can simultaneously observe and rapidly process an almost limitless number of inputs. Furthermore, these systems can learn from each incremental case and can be exposed, within minutes, to more cases than a clinician could see in many lifetimes. Artificial intelligence complements the vast number of digital images created in hospitals, the products of next-generation imaging scanners, especially hybrids that include MRI, CT, PET, and SPECT. In recent years, machine learning algorithms are rapidly being used in medical image analysis. These machine learning techniques are used to extract compact information to improve the performance of medical image analysis. Recently, deep learning methods using deep convolutional neural networks have been applied to medical image analysis to provide promising results.[22] The neural network model is shown in Figure 4 below.

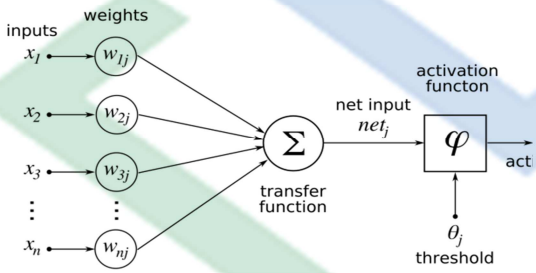

Figure 4. A neural network model.

Applications cover the full spectrum of medical image analysis, including detection, segmentation, classification, and computer-assisted diagnostics.[23] As a result, if artificial intelligence and healthcare professionals interact to accommodate deep thinking platforms, such as automation, in diagnosing a patient's disease state, artificial intelligence will play an important role in the analysis of medical image data, which will only be feasible.[24][25]

II. Experiment and result

For the experiment, we acquired T1 and T2 weighted images from The Cancer Imaging Archive site. The image was preprocessed to 256 x 256 pixels for segmentation and stored in a bitmap format. The stored images were segmented with 127 as the threshold. Six parameters per image were extracted from the segmented image using DWT. We learned neural networks by inputting extracted parameters into the neural networks. Figure 5 is a flow chart showing the whole process of the experiment.

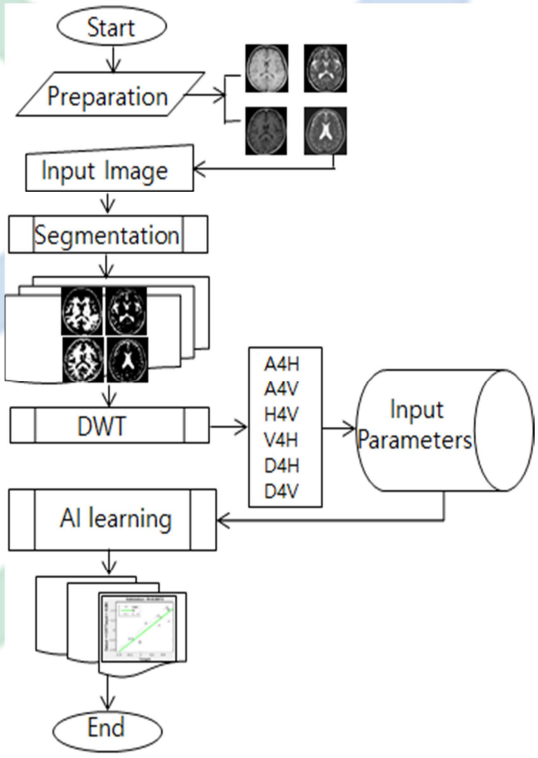

Figure 5 Flow-chart of experiment.

1. Image segmentation

Image segmentation plays an important role in many medical imaging applications by automating or

SJMI(2019) 01; 11-23

facilitating the depiction of anatomical structures and other areas of interest. We segmented the highlighted portion of the T1 weighted and T2 weighted images of the MRI image with a threshold of 127. Table 1 below shows the original and segmented images of the T1 and T2 weighted images.

Table 1. Segmentation images

	T1WI_1	T1WI_2	T2WI_1	T2WI_2
original image	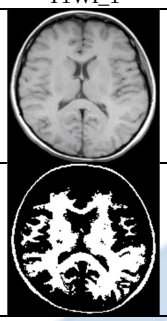	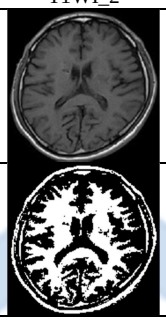	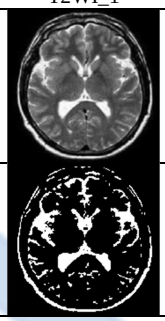	
segmented image				

2. Discrete Wavelet Transform

In numerical and functional analysis, the discrete wavelet transform (DWT) is any wavelet transform in which the wavelet is sampled discretely. As with other wavelet transforms, the main advantage over Fourier transforms is time resolution. We did MatLab programming to extract six feature parameters. The variable names of the extracted parameters are as follows:

A4H: Horizontal low frequency
A4V: Vertical Low Frequency
H4V: horizontal high frequency
V4H: vertical high frequency
D4H: horizontal diagonal high frequency
D4V: vertical diagonal high frequency

Tables 2 to 9 show extracted feature values by DWT from images of table 1.

Table 2. Feature extraction value of T1WI_1 original image

A4H	**-0.50**	**-0.49**	**-0.43**	**-0.21**	**-0.23**	**-0.12**	**0.07**	**0.15**	**0.26**	**0.31**	**0.39**	**0.44**	**0.49**	**0.50**	**0.49**	**0.42**
A4V	**-0.50**	**-0.47**	**-0.23**	**-0.31**	**-0.21**	**-0.07**	**0.05**	**0.14**	**0.19**	**0.28**	**0.37**	**0.38**	**0.37**	**0.43**	**0.48**	**0.50**
H4V	**-0.50**	**-0.47**	**-0.39**	**-0.25**	**-0.04**	**0.01**	**0.18**	**-0.01**	**-0.17**	**0.11**	**-0.23**	**0.15**	**0.17**	**-0.16**	**0.27**	**0.50**
V4H	**-0.50**	**-0.49**	**-0.43**	**-0.30**	**-0.20**	**-0.11**	**0.08**	**0.37**	**0.49**	**0.37**	**-0.08**	**0.35**	**0.19**	**-0.21**	**0.31**	**0.50**
D4H	**-0.50**	**-0.45**	**-0.22**	**0.06**	**0.50**	**0.27**	**0.06**	**-0.03**	**-0.25**	**-0.08**	**-0.12**	**-0.27**	**-0.38**	**-0.32**	**-0.24**	**-0.21**
D4V	**-0.50**	**-0.02**	**0.50**	**-0.06**	**0.00**	**0.02**	**0.09**	**0.22**	**0.49**	**0.19**	**-0.02**	**0.01**	**-0.12**	**-0.12**	**-0.15**	**-0.24**

Table 3. Feature extraction value of T1WI_1 segmental image

A4H	**-0.50**	**-0.49**	**-0.44**	**-0.29**	**-0.38**	**-0.38**	**-0.33**	**-0.23**	**-0.06**	**-0.14**	**0.03**	**0.43**	**0.50**	**0.47**	**0.14**	**-0.18**
A4V	**-0.50**	**-0.47**	**-0.26**	**-0.38**	**-0.42**	**-0.43**	**-0.44**	**-0.37**	**-0.02**	**0.22**	**0.50**	**0.36**	**-0.02**	**0.28**	**0.48**	**0.47**
H4V	**-0.50**	**-0.48**	**-0.42**	**-0.40**	**-0.35**	**-0.35**	**-0.29**	**-0.17**	**-0.07**	**0.06**	**-0.14**	**0.03**	**-0.07**	**-0.19**	**0.50**	**0.12**
V4H	**-0.50**	**-0.49**	**-0.47**	**-0.41**	**-0.38**	**-0.37**	**-0.08**	**0.10**	**0.50**	**0.15**	**0.08**	**-0.15**	**-0.27**	**-0.14**	**0.10**	**0.14**
D4H	**-0.50**	**-0.42**	**-0.11**	**0.09**	**0.18**	**0.17**	**0.27**	**0.42**	**0.04**	**0.50**	**0.42**	**-0.04**	**0.10**	**0.34**	**0.09**	**-0.12**
D4V	**-0.50**	**-0.19**	**0.01**	**-0.30**	**-0.17**	**-0.12**	**-0.01**	**0.50**	**0.18**	**-0.01**	**0.25**	**-0.14**	**0.15**	**0.38**	**-0.04**	**0.39**

Table 4. Feature extraction value of T1WI_2 original image

A4H	**-0.50**	**-0.50**	**-0.49**	**-0.34**	**-0.20**	**-0.13**	**-0.07**	**0.03**	**0.12**	**0.21**	**0.30**	**0.38**	**0.45**	**0.50**	**0.48**	**0.35**
A4V	**-0.50**	**-0.49**	**-0.33**	**-0.09**	**-0.19**	**-0.12**	**0.04**	**0.12**	**0.23**	**0.39**	**0.34**	**0.39**	**0.50**	**0.44**	**0.50**	**0.50**
H4V	**-0.50**	**-0.49**	**-0.43**	**-0.33**	**-0.21**	**-0.22**	**-0.10**	**-0.13**	**-0.23**	**0.50**	**-0.06**	**0.00**	**-0.28**	**0.28**	**0.46**	**-0.14**
V4H	**-0.50**	**-0.50**	**-0.47**	**-0.41**	**-0.20**	**-0.37**	**-0.06**	**-0.20**	**-0.11**	**-0.20**	**0.03**	**0.15**	**-0.05**	**0.10**	**0.50**	**0.23**
D4H	**-0.50**	**-0.48**	**-0.39**	**-0.06**	**0.16**	**0.20**	**0.50**	**0.22**	**0.13**	**0.03**	**-0.04**	**-0.10**	**-0.27**	**-0.16**	**-0.24**	**-0.26**
D4V	**-0.50**	**-0.45**	**-0.05**	**0.00**	**0.21**	**0.45**	**0.50**	**0.36**	**0.27**	**-0.05**	**-0.22**	**0.13**	**0.00**	**-0.05**	**0.17**	**-0.07**

Table 5. Feature extraction value of T1WI_2 segmental image

A4H	-0.50	-0.50	-0.48	-0.34	-0.32	-0.30	-0.22	-0.12	-0.07	0.09	0.24	0.39	0.43	0.50	0.50	0.18
A4V	-0.50	-0.48	-0.38	-0.21	-0.33	-0.36	-0.21	-0.08	0.05	0.26	0.18	0.30	0.50	0.27	0.42	0.39
H4V	-0.50	-0.49	-0.42	-0.33	-0.23	-0.15	-0.14	0.12	0.09	0.34	0.04	0.06	-0.20	0.10	0.50	0.15
V4H	-0.50	-0.50	-0.48	-0.42	-0.19	-0.32	-0.03	-0.03	0.21	0.48	0.08	0.42	-0.13	0.14	0.50	0.43
D4H	-0.50	-0.49	-0.42	0.01	0.12	0.12	0.50	0.15	0.43	0.29	0.41	0.28	-0.25	0.08	0.08	0.23
D4V	-0.50	-0.47	-0.23	-0.18	0.04	0.21	0.49	0.50	0.28	0.13	-0.14	0.24	-0.14	0.03	0.25	-0.11

Table 6. Feature extraction value of T2WI_1 original image

A4H	-0.50	-0.50	-0.50	-0.48	-0.33	-0.27	-0.16	0.05	0.40	0.50	0.36	0.38	0.41	0.35	0.36	0.33
A4V	-0.50	-0.50	-0.41	-0.29	-0.17	-0.03	0.04	0.09	0.16	0.08	0.05	0.16	0.40	0.50	0.41	0.36
H4V	-0.50	-0.49	-0.38	-0.32	-0.09	-0.01	0.11	0.19	0.26	0.10	0.34	0.47	0.33	0.44	0.44	0.50
V4H	-0.50	-0.50	-0.50	-0.47	-0.31	-0.18	-0.15	-0.26	-0.06	0.11	0.33	0.50	0.31	0.26	0.25	0.41
D4H	-0.50	-0.50	-0.49	-0.33	-0.20	0.17	0.21	-0.01	0.49	0.50	-0.03	-0.05	-0.18	-0.07	-0.09	0.15
D4V	-0.50	-0.41	-0.29	-0.19	-0.05	0.13	0.11	0.50	0.07	-0.17	0.04	0.42	0.31	-0.14	-0.19	-0.19

Table 7. Feature extraction value of T2WI_1 segmental image

A4H	-0.50	-0.50	-0.50	-0.49	-0.35	-0.34	-0.22	0.09	0.50	0.38	0.22	-0.01	-0.05	-0.36	-0.14	-0.05
A4V	-0.50	-0.49	-0.44	-0.37	-0.29	-0.04	-0.12	-0.17	0.00	-0.28	-0.20	0.05	0.45	0.50	0.32	0.35
H4V	-0.50	-0.48	-0.29	-0.29	0.01	0.01	-0.14	0.11	0.26	-0.09	0.36	0.50	0.41	0.29	0.18	0.32
V4H	-0.50	-0.50	-0.50	-0.47	-0.31	-0.31	-0.31	-0.30	-0.23	-0.11	0.44	0.50	0.26	-0.13	0.00	0.08
D4H	-0.50	-0.50	-0.50	-0.35	-0.25	0.13	-0.07	-0.02	0.34	0.50	0.30	0.47	0.03	-0.09	-0.19	0.23
D4V	-0.50	-0.40	-0.35	-0.20	-0.13	-0.08	-0.11	0.50	0.05	-0.12	0.13	0.34	0.10	-0.08	-0.12	-0.16

Table 8. Feature extraction value of T2WI_2 original image

A4H	-0.50	-0.50	-0.50	-0.46	-0.27	-0.26	-0.20	0.13	0.32	0.24	0.33	0.31	0.32	0.29	0.37	0.50
A4V	-0.50	-0.50	-0.48	-0.26	-0.02	0.21	0.24	0.21	0.23	0.30	0.31	0.29	0.50	0.47	0.38	0.45
H4V	-0.50	-0.49	-0.45	-0.41	-0.30	-0.03	0.01	0.07	0.19	-0.07	0.25	0.18	0.50	0.26	0.11	0.38
V4H	-0.50	-0.50	-0.50	-0.45	-0.37	-0.36	-0.27	0.02	0.50	0.37	0.04	0.17	0.32	0.02	0.34	0.37
D4H	-0.50	-0.48	-0.40	-0.15	-0.11	0.47	0.50	0.35	0.16	0.44	0.39	-0.01	-0.01	-0.04	0.24	0.27
D4V	-0.50	-0.45	-0.30	-0.18	0.50	0.40	-0.04	0.18	0.04	-0.18	-0.15	0.16	0.08	-0.01	0.10	0.18

Table 9. Feature extraction value of T2WI_2 segmental image

A4H	-0.50	-0.50	-0.50	-0.44	-0.13	-0.22	-0.14	0.33	0.50	0.15	0.16	-0.04	0.02	-0.04	0.18	0.36
A4V	-0.50	-0.50	-0.44	-0.13	0.26	0.35	0.24	0.08	0.01	0.06	-0.07	-0.02	0.50	0.37	-0.06	0.08
H4V	-0.50	-0.49	-0.45	-0.36	-0.20	0.13	0.01	0.12	0.09	-0.09	0.07	0.29	0.45	0.30	0.24	0.50
V4H	-0.50	-0.50	-0.49	-0.42	-0.36	-0.37	-0.27	-0.12	0.50	0.17	0.12	0.17	0.10	-0.08	0.32	0.16
D4H	-0.50	-0.50	-0.42	-0.17	-0.21	0.13	0.09	0.39	-0.07	0.29	0.50	-0.06	-0.10	-0.07	0.00	0.07
D4V	-0.50	-0.43	-0.13	0.01	0.36	0.50	0.25	0.19	-0.20	0.00	-0.02	0.08	0.09	0.14	0.15	0.16

3. Training of Neural Network

Deep learning neural network models learning to map inputs to outputs given a training dataset of experiments. The training process involves finding a set of weights in the network that proves to be good, or good enough, at solving the specific problem. This training process is iterative, meaning that it progresses step by step with small updates to the model weights each iteration and, in turn, a change in the performance of the model each iteration. The iterative training process of neural networks solves an optimization problem that finds for parameters that result in a minimum error or loss when evaluating the examples in the training dataset. In pattern recognition problems, we want a neural network to classify inputs into a set of target categories. The neural pattern recognition will help you select data, create and train a network, and evaluate its performance using cross-entropy and confusion matrices. Figure 6 shows the standard NARX(Nonlinear Autoregressive with External Input) network implemented for the experiment. The standard NARX(Nonlinear Autoregressive with External Input) network is a two-layer feedforward network with sigmoid transfer functions in the hidden layer and linear transfer functions in the output layer. The network also uses tap delay lines to store the previous values of the x (t) and

SJMI(2019) 01; 11-23

y (t) sequences. y(t) As a function of y(t – 1), y(t – 2), ..., y(t – d), the output y(t) of the NARX network is fed back to the network input via delay. However, we can open this feedback loop for efficient training. Since true outputs are available during network training, the open-loop architecture above uses the actual outputs instead of feeding back the expected outputs. This has two advantages. The first is that the input to the feedforward network is more accurate. The second is that the resulting network has a pure feedforward architecture, so more efficient algorithms can be used for training. The default number of hidden neurons is set to 10. The default number of delays is two.

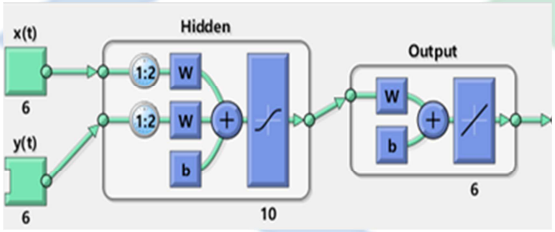

Figure 6. The neural network diagram

(1) Result of training to T1WI

We input the feature values extracted from two different T1-weighted original images into the neural network and trained them. The results of the training are shown in Figure 7.

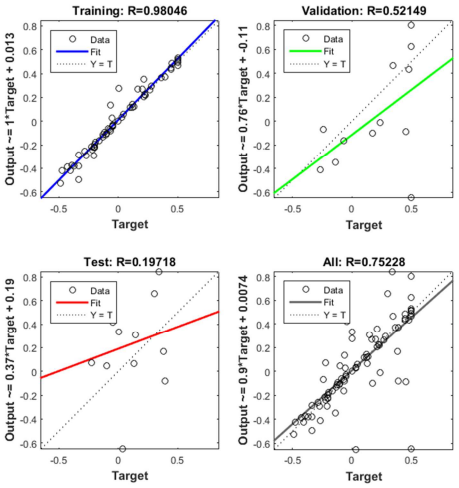

Figure 7. Regression of T1WI Original image

Figure 8 shows the results of training from the feature values extracted from two different T1 weighted segmented images into the neural network.

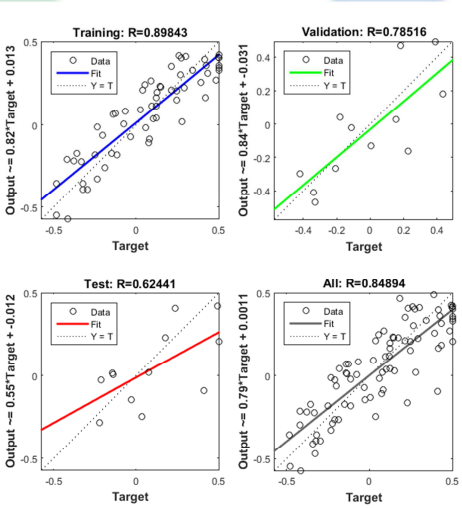

Figure 8. Regression of T1WI segmental image

(2) Result of training to T2WI

Figure 9 shows the results of training from the feature values extracted from two different T2 weighted original images into the neural network.

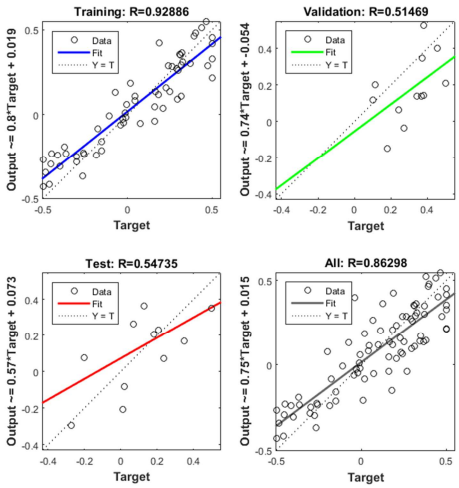

Figure 9. Regression of T2WI Original image

Figure 10 shows the results of training from the feature values extracted from two different T2 weighted segmental images into the neural network.

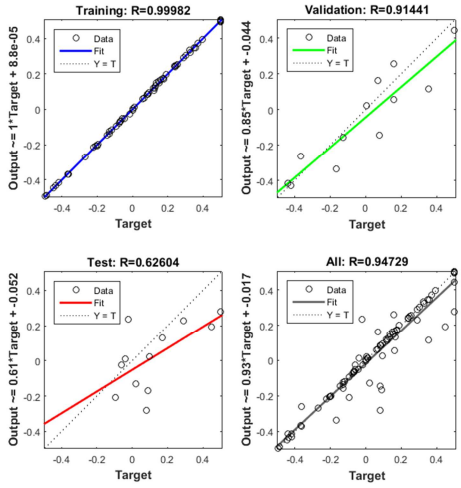

Figure 10. Regression of T2WI segmental image

(3) Result of training to T1WI and T2WI

Figure 11 shows the results of training from the feature values extracted from two different T1 and T2 weighted original images into the neural network.

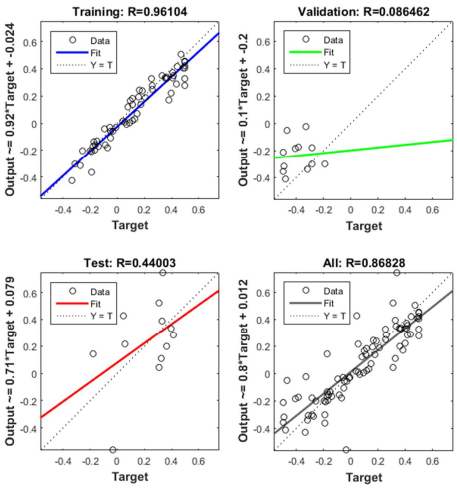

Figure 11. Regression of T1WI and T2WI Original image

Figure 12 shows the results of training from the feature values extracted from two different T1 and T2 weighted segmental images into the neural network.

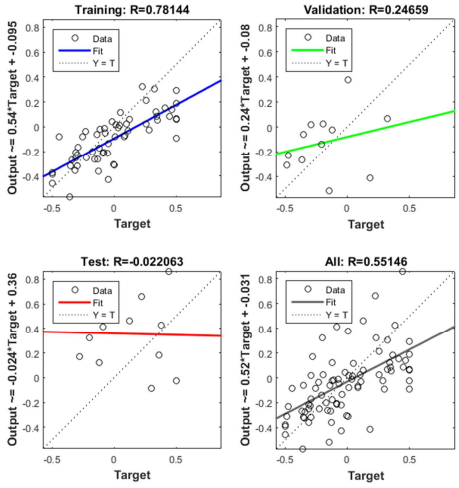

Figure 12. Regression of T1WI and T2WI segmental image

III. Results and discussion

To check the pattern of the extracted feature values, the graphs are shown in Figure 13 ~ 16. It can be seen that the pattern of the original

SJMI(2019) 01; 11-23

image and the segmented image are similar. The similarity of patterns suggests that segmented images typically have shape values. Therefore, if the shape value of the segmented image is used as the input value of the neural network, the learning time will be shortened and the accuracy of the learning result will be increased.[26]

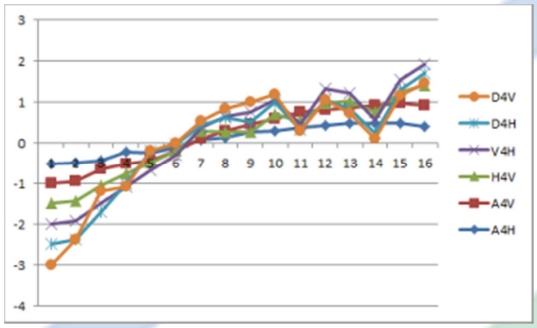

(a) Originally

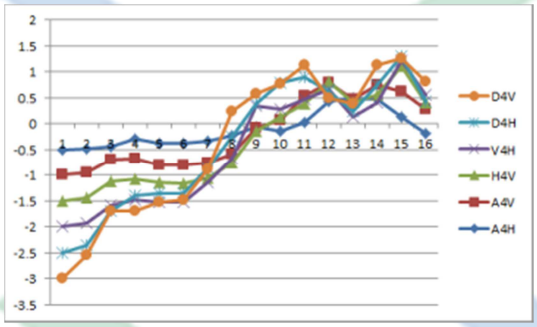

(b) Segmented

Figure 13. Feature graph of T1WI_1 Image

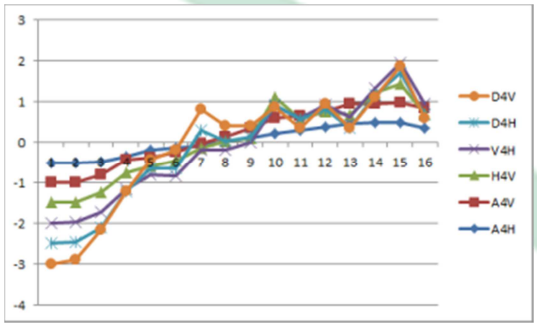

(a) Originally

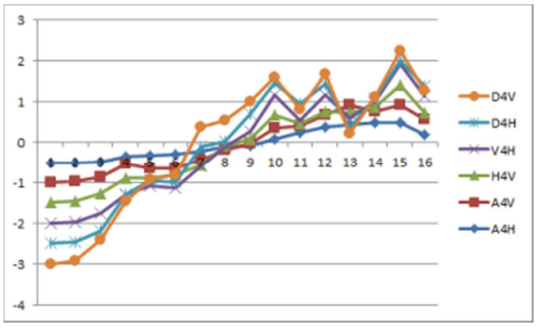

(b) Segmented

Figure 14. Feature graph of T1WI_2 Image

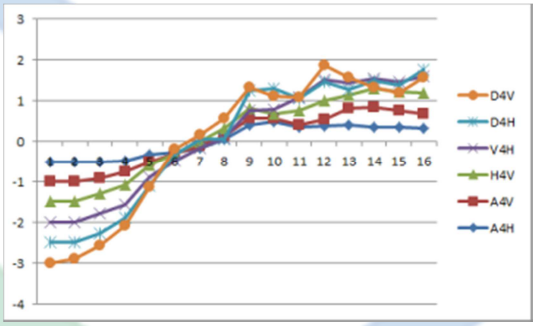

(a) Originally

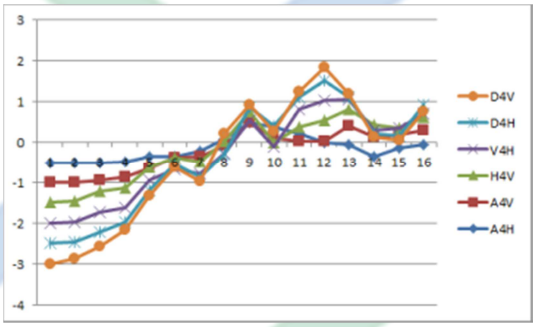

(b) Segmented

Figure 15. Feature graph of T2WI_1 Image

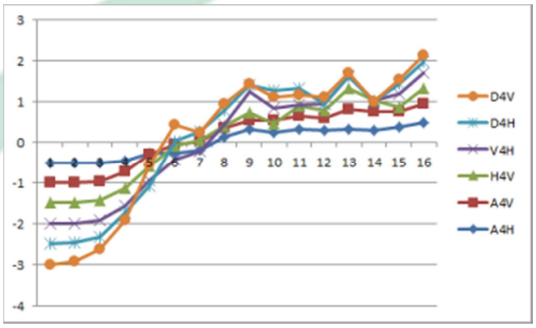

(a) Originally

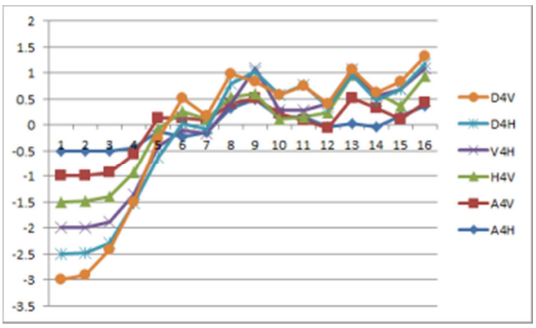

(b) Segmented

Figure 16. Feature graph of T2WI_2 Image

To evaluate the similarity between two images, the neural network was trained as follows input data : (1) Pair of T1 weighted original image, (2) Pair of T1 weighted segmental image, (3) Pair of T2 weighted original image, (4) Pair of T2 weighted segmental image, (5) T1 and T2 weighted original image, (6) T1 and T2 weighted segmental image. Figure 17 shows R values corresponding to training, validation, test, and all.

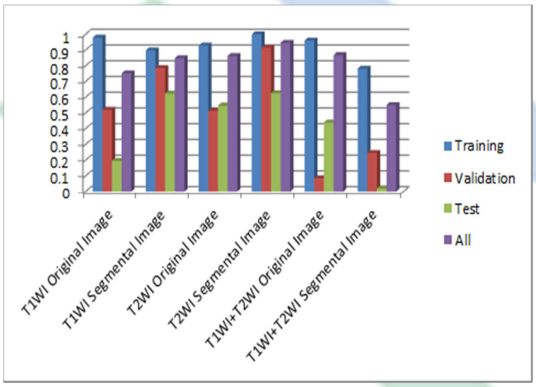

Figure 17. R-value of after running the neural network

Figure 17 shows R-values corresponding to training, validation, test, and all. In Figure 17, it can be seen that the R-value of the segmented image is closer to 1 than the original image. The reason for this is that the image obtained by segment the region of the weighted portion already has similarities. Also, it can be seen that the similarity between the T1 and T2 weighted images is high in the same combination, and that the similarity is relatively low in the different weighted images. If we improve the learning result of the neural network and use the result of this study, we can classify the magnetic resonance image automatically.

IV. Conclusion

In this study, we proposed a method to automatically classify MRI images by neural network learning. To this end, we segmented the weighting domain of MRI. In feature extraction, the original image and segmented image were extracted by DWT, respectively. A neural network was trained by inputting extracted feature values.

As a result of the experiment, it was found that the R-value of the segmented image is closer to 1 than the original image. The reason is that the images obtained by segmenting the areas of the weighted parts already have similarities. Also, it was found that the similarity between T1 and T2 weighted images is high in the same combination, and the similarity is relatively low in different weighted images. Improving the learning results of neural networks and using this study will be able to automatically classify MR images.

Artificial intelligence must break down barriers to be widely accepted and reliable in mainstream medical imaging environments. This is because validation studies are needed to demonstrate the performance of deep learning algorithms in clinical environments.

The most important issue in medical imaging is ensuring the confidence of radiologists using artificial intelligence. To solve this problem, it is of utmost importance that the algorithm developer and radiological technologist work together to provide a solution that is integrated with the radiologist's workflow.

[Reference]

[1] Dietrich Harder, "***Röntgen's Discovery–How and Why It Happened***", International Journal of Radiation Biology and Related Studies in Physics, Chemistry and Medicine, 1987, Volume 51, issue 5, pp. 815~839.

[2] Paulo Leitao, Armando Walter Colombo, Stamatis Karnouskos, "***Industrial automation based on cyber-physical systems technologies: Prototype implementation and challenges***", 2016, Computers in Industry, Volume 81, PP. 11~25.

[3] Antonio dos Anjos, Hamid Reza Shahbazkia, "***Bi-Level Image Thresholding A Fast Method***", In Proceedings of the First International Conference on Bio-inspired Systems and Signal Processing, pages 70-76, DOI: 10.5220/0001064300700076.

[4] HeikoAndra, NicolasCombaret, JackDvorkin, ErikGlatt, et al, ""***Digital rock physics benchmarks-Part I: Imaging and segmentation***", 2012, Computer & Geosciences, Volume 50, PP. 25~32.

[5] M. Lalitha, M. Kiruthiga, C. Loganathan, "***A Survey on Image Segmentation through Clustering Algorithm***", 2013, IJSR, Volume 2, Issue 2, PP. 348~358.

[6] Koushik Mondal, Paramartha Dutta, Siddhartha Bhattacharyya, "***Fuzzy Logic Based Gray Image Extraction and Segmentation***", 2012, International Journal of Scientific & Engineering Research, Volume 3, Issue 4, PP. 1~14.

[7] Om Prakash, Ashish Khare, "***Tracking of moving object using energy of biorthogonal wavelet transform***", 2015, Chiang Mai J. Sci, Volume 42. No. 3, pp. 783~795.

[8] Ilkay Darilmaz, "***Wavelet Based Similarity Measurement Algorithm for Seafloor Morphology***", 2006, MIT, Master of Science in Mechanical Engineering, pp. 24~52.

[9] Juuso Olkkonen, "***DISCRETE WAVELET TRANSFORMS – THEORY AND APPLICATION***", 2011. Books.google.com, pp181~256.

[10] Eric J. Topol, "***High-performance medicine: the convergence of human and artificial intelligence***", 2019, nature medicine, volume 25 pp. 44~56.

[11] Wang, X. et al. "***ChestX-ray8: hospital-scale chest X-ray database and benchmarks on weakly-supervised classification and localization of common thorax diseases***.", 2017, Preprint at https://arxiv.org/abs/1705.02315.

[12] Steve G. Langer, Stephen J. Carter, David R. Haynor, et al, "***Image Acquisition: Ultrasound, Computed Tomography, and Magnetic Resonance Imaging***", 2001, World J Surg 25, pp. 1428–1437,

doi:10.1007/s00268-001-0128-y.

[13] Nam, J. G. et al. "***Development and validation of deep learning–based automatic detection algorithm for malignant pulmonary nodules on chest radiographs***", 2018, Radiology, https://doi. https://doi.org/10.1148/radiol.2018180237.

[14] Vojislav Kecman, "***Learning and Soft Computing***", 2001, The MIT Press, pp. 255~393.

[15] Daniel S. W. Ting, Yong Liu, et al, "***AI for medical imaging goes deep***", 2018, nature medicine, volume 24, pp. 539~540.

[16] AnantMadabhushi, GeorgeLee, "***Image analysis and machine learning in digital pathology: Challenges and opportunities***", 2016, Medical Image Analysis, Volume 33, pp. 170~175.

[17] Ahmed Hosny, Chintan Parmar, et al. "***Artificial intelligence in radiology***", 2018, nature reviews cancer, volume 18 pp. 500~510.

[18] Kun-Hsing Yu, Andrew L. Beam, Isaac S. Kohane, "***Artificial intelligence in healthcare***", 2018, nature biomedical engineering, volume 2, pp. 719~731.

[19] GangWang, T.WarrenLiao, "***Automatic identification of different types of welding defects in radiographic images***", 2002, NDT & E International, Volume 35, Issue 8, pp. 519~528.

[20] Klaus Schwab, "***The fourth industrial revolution***", 2016, books.google.com, pp. 1~25.

[21] I L Pykett, J H Newhouse, F S Buonanno, T J Brady, et al, "***Principles of nuclear magnetic resonance imaging***", Radiology, 1982, Vol. 143, No. 1, PP. 157~168.

[22] Satish Kumar, Raghavendra Srinivas, "***A Study on Image Segmentation and its Methods***", 2013, International Journal of Advanced Research in Computer Science and Software Engineering, Volume 3, Issue 9, pp. 1112~1114.

[23] P. Natarajan, N Krishnan, Natasha Sandeep Kenkre, et al, "***Tumor detection using threshold operation in MRI brain images***", 2012 IEEE International Conference on Computational Intelligence and Computing Research, DOI: 10.1109/ICCIC.2012.6510299.

[24] Marina E. Plissiti, Christophoros Nikou, Antonia Charchanti, "***Combining shape, texture and intensity features for cell nuclei extraction in Pap smear images***", 2011, Pattern Recognition Letters, Volume 32, Issue 6, PP. 838~853.

[25] I. Carlbom, D. Terzopoulos, K.M. Harris, "***Computer-assisted registration, segmentation, and 3D reconstruction from images of neuronal tissue sections***", 1994, IEEE Transactions on Medical Imaging, Volume 13, Issue 2, pp. 351~362.

[26] Zheng Liu, Hiroyuki Ukida, Pradeep Ramuhalli, Kurt Niel, "***Integrated Imaging and Vision Techniques for Industrial Inspection***", 2015, Springer, pp. 319~412, DOI : doi.org/10.1007/978-1-4471-6741-9.